THE JOURNAL OF PHYSICAL CHEMISTRY C
A JOURNAL OF THE AMERICAN CHEMICAL SOCIETY

pubs.acs.org/JPCC
Article

Insights into the Rate-Determining Step of the Ethanol Electro-oxidation Reaction on the Pd(111) Surface through Ab Initio Molecular Dynamics Simulations

Jonathan Campeggio, Walter Giurlani, Marco Pagliai, Massimo Innocenti, Claudio Fontanesi, and Riccardo Chelli*

Cite This: J. Phys. Chem. C 2023, 127, 21075−21084
Read Online

ABSTRACT: The ethanol electro-oxidation mechanism on a Pd(111) surface in alkaline media has been studied through ab initio molecular dynamics simulations. It is known that, under these conditions, ethanol undergoes partial oxidation to acetate and that hydroxylation of the acetyl radical plays a fundamental role in the overall reaction kinetics. Therefore, we focused on this reaction step, specifically addressing the interplay of the acetyl and hydroxyl radicals and especially the effect of their arrangement over the Pd surface on the hydroxylation process. We observed that the strength of the interactions of the reacting species with the Pd surface significantly modulates the propensity of the reaction. In fact, for minimum-energy arrangements of the acetyl-surface and OH-surface systems, hydroxylation appears hindered by the strong interactions between the surface and substrates, while it readily takes place when the substrates are moved away from the surface. These results open to the idea of rational design of cocatalysts based on the tuning of surface chemical properties addressed to weaken the adsorbate/adsorbent interactions, eventually enhancing the exchange current density.

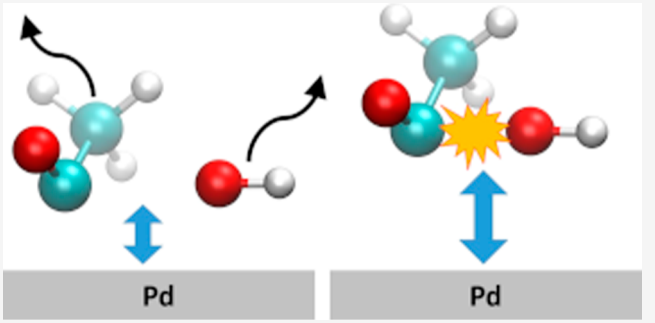

1. INTRODUCTION

In the last years, direct-ethanol (EtOH) fuel cells emerged as a promising technology for power generation because they can provide electric energy in an efficient way with negligible emission of polluting products.[1,2] EtOH has several advantages over hydrogen and methanol, the other two compounds extensively studied for the same purpose. It is much less toxic and less volatile than methanol, and its storage and transport are safer than hydrogen. In addition, EtOH can be produced in large quantities from biomass and agricultural waste.[1]

In direct EtOH fuel cells, EtOH is oxidized at the anode, while the oxygen reduction reaction occurs at the cathode. In principle, the complete oxidation of EtOH to CO_2 gives higher energy density than H_2 oxidation since it can deliver 12 electrons per molecule. In practice, partial oxidation to acetic acid (acetate into alkaline media) occurs and only 4 electrons per molecule are delivered.[3−6] The EtOH oxidation reaction (EOR) occurs only when promoted by a proper catalyst. Among the many tested catalysts, those based on Pd in alkaline media were found to be very effective.[5,7,8] For example, Ma et al. showed that the apparent activation energy for EOR on Pd at basic pH is significantly lower than that observed on Pt in acid conditions.[9] Furthermore, alkaline electrolytes have the advantage of providing an environment in which transition metals, rare-earth metals, and oxides can be used as cocatalysts to promote the catalytic activity of Pd-based electrodes.[5,10−15]

The EOR mechanism has not been completely characterized, but it has been ascertained that EOR involves some steps.[5] In the literature, several hypotheses, based on experimental[4,6,16−18] and theoretical[4,19−25] studies, have been proposed. Two theoretical pathways leading to CO_2 or acetate, often termed C1 and C2 pathways, respectively, have been reported. In both cases, after the adsorption of the EtOH molecule on the Pd(111) surface, the first dehydrogenation step occurs in the methylene group. Then, two competitive routes, leading, in turn, to 1-hydroxyethylidene (CH_3COH) and acetaldehyde (CH_3CHO) can occur. Both intermediates, however, converge to acetyl (CH_3CO), which can evolve toward either the C1 or C2 pathways, through a C−C bond breaking (C1) or a hydroxylation process (C2). The occurrence of acetyl during the EOR pathway has been

Received: July 7, 2023
Revised: October 3, 2023
Published: October 18, 2023

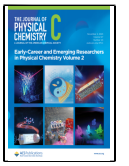

https://doi.org/10.1021/acs.jpcc.3c04587
J. Phys. Chem. C 2023, 127, 21075−21084

revealed in several experimental studies and has been considered as a key intermediate in theoretical analysis.[4,25,26]

Furthermore, the pivotal role of acetyl in determining the EOR rate has also been outlined with experimental techniques like in situ attenuated total reflection surface-enhanced infrared absorption and density functional theory (DFT) calculations.[18,25,26] In particular, it has been hypothesized that acetyl hydroxylation

$$CH_3CO + OH \rightarrow CH_3COOH \quad (1)$$

is the rate-determining step of the oxidation process of EtOH.[18,27]

In a previous article[28] by some of us, the α-hydrogen extraction of EtOH performed by the hydroxyl radical on the Pd(111) surface has been studied through quantum mechanical methods, highlighting the importance of the mutual arrangement of reacting species and Pd surface in modulating the reaction rate.

In the present study, we apply the approach employed in ref 28 to the key reaction step, eq 1, occurring on Pd layers assembled along the (111) direction. Specifically, this reaction has been investigated by ab initio molecular dynamics (AIMD) simulations modulating both the distance between the two reacting species, namely, CH_3CO and OH, and the distance between these molecules and the Pd surface. The simulation trajectories reveal that the distance of the reactants from the surface plays a key role in the kinetics of the process. In particular, we observe that the most reactive trajectories are featured by long distances, corresponding to low interaction energies between reactants and the Pd surface.

2. COMPUTATIONAL METHODS

Quantum mechanical calculations were carried out using DFT. In particular, we performed (a) a series of energy-based geometry optimizations of the acetyl and acetyl-OH assembly on the Pd(111) surface in order to estimate their adsorption and coadsorption energies, respectively, and (b) Born–Oppenheimer molecular dynamics simulations to identify the propensity of the acetyl hydroxylation reaction (eq 1) in dependence of the mutual arrangement of acetyl and OH on the Pd surface. Calculations have been performed with the Quickstep module of the CP2K suite of programs.[29,30]

The Perdew–Burke–Ernzerhof (PBE) functional[31] has been used to treat the exchange–correlation energy along with the Grimme D3 correction[32] to account for the dispersion interactions. The electronic structure has been computed by means of the Gaussian and plane-wave approach, with the core region of each atom described through Goedecker–Teter–Hutter (GTH) pseudopotentials.[33,34] In particular, GTH-PBE-q6, GTH-PBE-q1, GTH-PBE-q4, and GTH-PBE-q18 pseudopotentials have been employed for the O, H, C, and Pd atoms, respectively (the last part of the pseudopotential name indicates the number of valence electrons). The electron density has been modeled by using a plane-wave cutoff of 500 Ry and a relative cutoff of 80 Ry, whereas the wave function has been described through the DZVP-MOLOPT-GTH Gaussian basis set. For the Pd atom, the short-range version of this basis set has been employed.[35] All calculations performed on the acetyl-surface system are open-shell (doublet spin multiplicity), while when both acetyl and OH radicals enter the calculation, namely, in the geometry optimizations of the acetyl-OH assembly on the Pd surface and in the AIMD simulations, a singlet spin state has been enforced to preserve the spin multiplicity. We note, in fact, that the reaction product is acetic acid, namely, a species with singlet spin multiplicity.

The Pd surface has been prepared from a .cif file containing the experimental atomic coordinates at 298 K.[36,37] The unit cell has been transformed to show the (111) surface on the xy plane, using the VESTA package.[38] The metal slab consists of 2 × 3 unit cells along the xy plane, and therefore, the system has periodicity along the x and y directions. Accordingly, periodic boundary conditions have been applied with an x, y periodicity of 9.529 × 8.252 Å. The metal surface is thus formed by 48 Pd atoms distributed in four layers parallel to the xy plane, with 2.246 Å being the distance between adjacent planes. In principle, the system does not have periodicity along the z direction. Nevertheless, in order to speed up the calculations, we have also enforced periodic boundary conditions in the z direction with an arbitrarily long periodicity, i.e., 30 Å, a size large enough to avoid interactions among the images. However, despite the modest dimensions of the acetyl and OH molecules, such spurious interactions cannot be excluded a priori, especially for those images arranged in the xy plane. Therefore, to verify the absence of artifacts due to the periodic boundary conditions in the x and y directions, we have repeated two representative AIMD simulations by doubling, in turn, the box side lengths in the x and y directions. In particular, we chose to repeat the two simulations leading one to a reactive path (acetyl hydroxylation) and the other to a nonreactive path. Overall, we noted negligible changes in the system trajectories. Details on these control calculations are reported in Section 1 of the Supporting Information. Since Pd is a metal conductor, the smearing technique according to the Fermi–Dirac distribution (300 K electronic temperature) was adopted to handle the electronic properties. The number of additional molecular orbitals is 50.

In order to reduce the computational time of the ab initio geometry optimizations, we first performed energy-based structural optimizations using the semiempirical approach called the Geometry, Frequency, Noncovalent, eXtended Tight Binding (GFN-xTB) method.[39] Optimizations have been carried out taking the bottom two layers in their bulk positions fixed, while the uppermost two layers and the adsorbates were fully relaxed without any constraints. These structural optimizations basically led to two minimum-energy arrangements of the acetyl radical on the Pd surface, which have been further optimized using DFT, adopting the settings described above. In both the semiempirical and DFT calculations, the orbital transformation method by VandeVondele and Hutter[40,41] has been adopted for wave function optimization. The adsorption energy of acetyl has been computed by subtracting the energy of the minimum-energy acetyl-surface system with the C_α atom constrained to a large distance from the surface (a distance, say d_∞, at which the interaction between acetyl and surface is negligible) to the energy of the minimum-energy nonconstrained acetyl-surface system estimated as described above. We point out that the zero-point vibrational energies have not been accounted for in the calculation. However, such a contribution to the adsorption energy is expected to be negligible, since a frequency shift upon adsorption as large as 1000 cm^{-1} yields an energy change of only ~1.4 kcal mol^{-1}, namely, about 2%, or less, of the adsorption energies into play. In order to estimate d_∞, we carried out a series of single-point DFT calculations. In these calculations, the arrangements of the Pd surface and acetyl have been fixed to those obtained from the DFT geometry

https://doi.org/10.1021/acs.jpcc.3c04587
J. Phys. Chem. C 2023, 127, 21075−21084

optimizations. In particular, taking fixed the mutual orientation of acetyl and surface as well as the geometries of acetyl and surface, single-point energy calculations have been carried out by progressively increasing the acetyl-surface distance, until reaching an almost constant energy trend. In addition to the determination of the d_∞ distance, estimated around 7.6 Å, useful to compute the adsorption energy of acetyl as discussed above, these calculations also provide a reliable estimate of the dependence of the interaction energy on the acetyl-surface distance, which turns out to be useful for the interpretation of the reactivity between acetyl and OH radicals on the Pd surface, eq 1. The coadsorption energy of the acetyl-OH molecular assembly on the Pd surface has been also estimated using an approach similar to that adopted for the acetyl. Basically, we evaluated the difference between two energies: the energy of a system formed by the three isolated species, namely, acetyl, OH and surface, has been subtracted from the energy obtained by optimizing the acetyl-OH assembly on the Pd surface. The former energy has been computed by a DFT geometry optimization enforcing a constraint to the C_α atom and to the hydroxyl O atom. The acetyl has been constrained at a d_∞ distance of 7.6 Å from the uppermost Pd layer (exactly the same distance employed to compute the adsorption energy of the acetyl alone), while OH has been constrained at a d_∞ distance of ∼14.8 Å from the uppermost Pd layer, shifted on the *xy* plane with respect to the acetyl. The resulting distance between the acetyl group and OH is ∼7.2 Å. This arrangement is consistent with a system formed by isolated species. In fact, as shown for the acetyl-surface system (see discussion of Figure 2), for distances above 6 Å, the residual interaction, dominated by dispersive forces, is negligible.

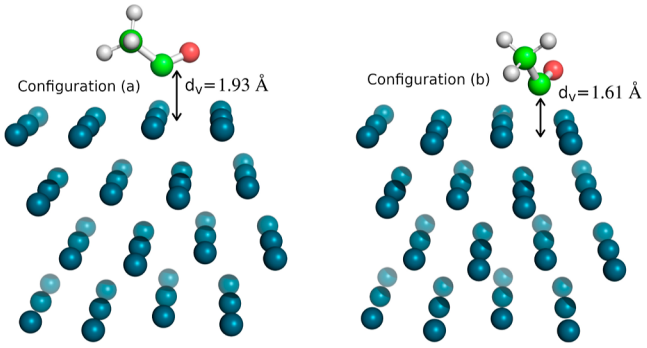

Figure 1. Ball and stick representations of the two minimum-energy arrangements of acetyl on the Pd surface obtained by DFT calculations. The distance of the C_α atom from the uppermost Pd layer, d_v, is reported. Periodic boundary conditions are applied: box side lengths along *x*, *y*, and *z* are 9.529, 8.252, and 30.000 Å, respectively, the *z* direction being perpendicular to the surface.

As stated above, reaction 1 is the main target of the present study, which has been addressed through AIMD simulations using microcanonical-ensemble (NVE) equations of motion with standard periodic boundary conditions. Note that all simulations presented here do not describe a system at equilibrium. Therefore, talking about sampling in the NVE ensemble does not make sense. In this respect, we point out that the NVE equations of motion, at variance with the canonical (NVT) equations of motion that exploit the coupling between the physical system and an unphysical thermostat, evolve the system without any external perturbation. Several simulations have been performed, differing from each other for

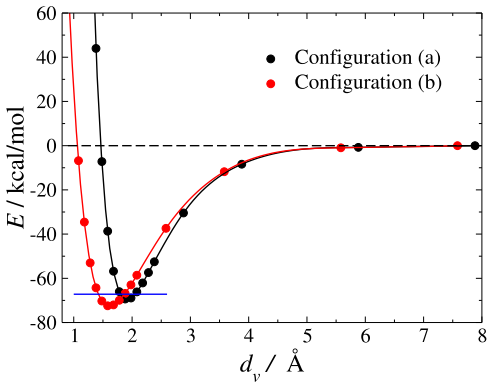

Figure 2. DFT energy scan at fixed configurations, specifically (a,b) of Figure 1, as a function of d_v, i.e., the distance between the C_α atom and the uppermost Pd layer. The curves are shifted to match the zero energy at the plateau, denoted as a dashed line. The adsorption energy, computed as described in the text, is indicated with a blue line for comparison. The calculated energies are reported with filled circles, while the solid lines are guides for the eyes.

the initial arrangement of the acetyl and OH molecules on the Pd surface. Specifically, keeping fixed the mutual orientation of acetyl and OH, their distance from the Pd surface, and/or the distance between acetyl and OH are set to different values in the initial configuration to probe the occurrence of reaction 1 in terms of these two configurational parameters. The system setup is further detailed in Section 3.2. Each simulation starts with all atoms at rest to eventually evaluate which initial configuration leads to the reaction product. During the simulations, in order to speed up the convergence of the self-consistent field calculation of the wave function, all the Pd atoms have been constrained to their bulk positions. Given the very short simulation times (none is longer than 250 fs), such an assumption is not expected to affect the qualitative trend in the results. Clearly, at the beginning of the simulation, a lot of potential energy is converted to kinetic energy, yielding global system heating. Therefore, to prevent uncontrollable heating of the reactive species during the dynamics, a threshold temperature of 1300 K has been enforced. When the temperature exceeds this threshold, the atomic velocities are uniformly scaled to cool the system to 300 K. A simulation run is stopped after establishing whether or not reaction 1 has occurred according to the geometrical criteria detailed in Section 3.2. Thus, the various simulation runs have different lengths, ranging between 150 and 250 fs. The time step used to integrate the equations of motion is 0.2 fs.

3. RESULTS AND DISCUSSION

3.1. Adsorption Energy of the Acetyl on the Pd Surface. Energy-based geometry optimizations of the acetyl on the Pd(111) surface were performed using the approach described in Section 2. In principle, several relative minimum-energy arrangements of the acetyl on the Pd surface may feature the system. Therefore, in order to address such a possibility, a series of GFN-xTB geometry optimizations have been carried out, starting from different initial configurations. All optimizations basically led to two prevalent structural motifs, in which the C_α atom of acetyl points toward the Pd surface and the CCO plane is nearly perpendicular to the surface. Representative configurations of these two structural motifs were employed in turn as input for further DFT geometry optimizations, obtaining modest rearrangements

https://doi.org/10.1021/acs.jpcc.3c04587
J. Phys. Chem. C 2023, 127, 21075−21084

with respect to the GFN-xTB geometries. Ball and stick representations of the minimum-energy arrangements obtained by DFT are shown in Figure 1.

An important difference between the two arrangements, denoted as configurations (a) and (b) in the figure, relies on the distance of the C_α atom from the Pd surface, namely, the d_v distance in Figure 1. This distance differs by more than 0.3 Å in the two configurations, being 1.93 and 1.61 Å in the (a) and (b) cases, respectively. This is basically due to the arrangement of the C_α atom above the uppermost Pd layer. In the (a) configuration, the C_α atom is located above a Pd atom in a nearly eclipsed configuration, while in the (b) configuration, the C_α atom forms a bridge-type structure together with two Pd atoms of the uppermost layer. The latter arrangement allows for a closer packing structure that, however, does not affect significantly the distance between the C_α atom and the first neighbor Pd atoms. In fact, in the (a) configuration there is one neighbor Pd atom at 1.97 Å, while in the (b) configuration, there are two equivalent neighbor Pd atoms at 2.10 Å.

Despite the structural differences outlined above, the two configurations are almost equivalent energetically, with the energy difference being as small as 0.01 kcal mol^{-1}. In this respect, we point out that the DFT energy accuracy with present available functionals is around 2 kcal mol^{-1}.[42] This implies that the adsorption energies associated with the two configurations are also almost identical. As a matter of fact, different minimum-energy arrangements of the type observed in the present work were also found in previous studies,[22,43] with energies differing by less than 1 kcal mol^{-1}.[22]

As discussed in Section 2, to compute the adsorption energy of the acetyl, both the minimum energy of the system and the energy of the noninteracting acetyl-surface system must be determined. For the latter calculation, the acetyl must be constrained at a distance from the surface large enough to prevent acetyl-surface interactions (we arbitrarily chose to fix the C_α atom). To roughly estimate such a distance, we have carried out a series of DFT single-point energy calculations varying the d_v distance while taking fixed the acetyl-surface arrangement as resulting from the structural optimizations discussed above. In practice, we have rigidly shifted the acetyl along the normal to the Pd surface. The energy *vs* d_v trend obtained from the two configurations is reported in Figure 2. The curves have been shifted to match the zero energy at the plateau. Therefore, the energy at the minimum corresponds to the acetyl-surface interaction energy evaluated at the fixed (optimized) geometry of the acetyl-surface system. From the two curves, we infer that the acetyl-surface interaction energy in the (b) configuration is greater than that in the (a) configuration by about 3 kcal mol^{-1}. This implies that as the relaxed structure of the system at large d_v is unique, a greater structural deformation features the (b) configuration upon adsorption. This could be justified by the fact that the closer packing featuring the (b) configuration globally yields a stronger interaction between the acetyl and surface. Nevertheless, this additional stabilization is counterbalanced by an almost equivalent loss of energy arising from the structural deformation of acetyl and surface. On the other side, in the (a) configuration, the acetyl does interact less strongly with the surface, leading to a smaller system deformation.

In summary, we note that a stronger interaction of the acetyl with the surface, as observed in the (b) configuration, leads to an energy gain upon binding but at the same time gives an energy loss due to a larger structural deformation of the system. Exactly the opposite occurs in the (a) configuration, in which a weaker acetyl-surface interaction is established. It is worth noting that these opposite effects counterbalance each other, making the two binding sites almost equivalent from the energetical standpoint. This may suggest that, assuming the strength of interaction as a dominant factor in the kinetics of the acetyl hydroxylation (eq 1), the EOR could be distributed almost homogeneously on the Pd surface, without the presence of any preferential reaction site.

As stated above, the evaluation of the d_v distance at which the energy plateau is reached (see Figure 2), allows us to perform a geometry optimization of the system in the absence of acetyl-surface interaction and hence to determine the structural relaxation contribution to the adsorption energy. In particular, we carried out a geometry optimization of the system by constraining d_v at 7.6 Å. Subtracting the corresponding energy to that of a (a) or (b) minimum-energy configuration allows us to recover the adsorption energy of that configuration including the structural relaxation. The resulting value amounts to −67.2 kcal mol^{-1} for both (a) and (b) configurations, since, as outlined above, their energies are nearly coincident. The adsorption energy is reported as a blue line in Figure 2 for comparison.

The adsorption energy obtained in the present study is lower by about 21 and 17 kcal mol^{-1} with respect to the values estimated by Pallassana and Neurock[43] and by Li and coworkers,[22] respectively. As pointed out by Tereshchuk and Da Silva,[44] this discrepancy could be ascribed to the van der Waals energy contribution, whose general effect is to enhance the molecule−surface interaction. In order to verify this observation, we repeated DFT energy optimizations of the acetyl-surface system in the absence of van der Waals interactions, starting from the bound and unbound arrangements of the (b) configuration of Figure 1 (d_v = 1.61 and 7.6 Å, respectively), obtained through optimization runs that include the van der Waals interactions. Our calculations partially confirm the Tereshchuk and Da Silva's[44] conclusions, as we obtained an adsorption energy of −56.6 kcal mol^{-1}, a value lower by only ∼6 and ∼10 kcal mol^{-1} with respect to the values obtained in refs 22 and 43.

The adsorption energy for the acetyl is comparable to that obtained for the OH, i.e., about −71.3 kcal mol^{-1}, by using the same level of theory.[28] The strong interaction between the acetyl and OH radicals and the Pd surface supports the hypothesis that the removal of the acetyl from the Pd surface by the hydroxyl radical (eq 1) is the rate-determining step of the EOR. Although the two reacting species show separately a large affinity with the Pd surface, assessing the effect of their mutual interaction on the adsorption features of the acetyl−OH assembly is mandatory. To this aim, we have estimated the coadsorption energy of acetyl and OH as described in Section 2. The minimum-energy geometry of the acetyl-OH assembly on the Pd surface is displayed in Figure 3. In this multibody interaction, the arrangement of the acetyl and OH molecules on the surface does not differ significantly from that observed in the absence of coadsorbed species. In fact, the C_α atom of the acetyl lies above a Pd atom (Pd^C in Figure 3), in a very similar way to the (a) configuration (see Figure 1). Also, the distance between the atoms C_α and Pd^C is nearly equal to that observed in the (a) configuration, namely, 1.98 Å against 1.97 Å. Analogously, the arrangement of the OH radical is not significantly affected by the presence of acetyl. Like in the

https://doi.org/10.1021/acs.jpcc.3c04587
J. Phys. Chem. C 2023, 127, 21075−21084

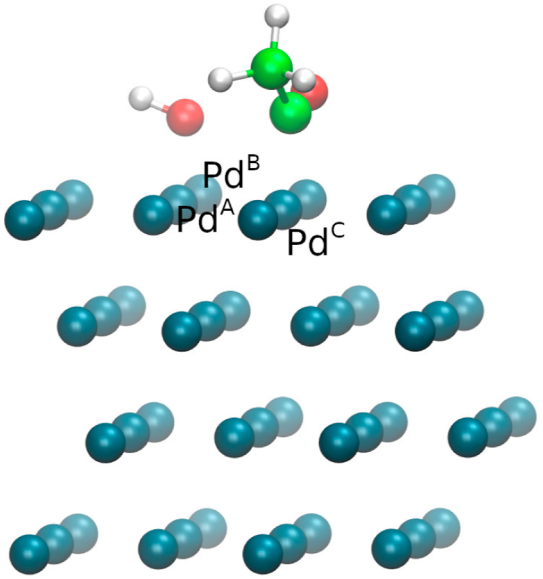

Figure 3. Ball and stick representation of the minimum-energy geometry of the acetyl-OH assembly on the Pd surface obtained by DFT calculations. The C_α atom lies nearly above the Pd^C atom. The hydroxyl O atom lies above the axis connecting the Pd^A and Pd^B atoms

absence of coadsorbed species, OH forms a bridge-type structure together with the Pd^A and Pd^B atoms (see also Figure S4 of the Supporting Information of ref 28), with a distance of 1.65 Å from the uppermost Pd layer (against 1.62 Å found in the absence of coadsorbed species[28]). In spite of the almost irrelevant effect of coadsorption on the structural features of the single adsorbed species, a more significant impact has been revealed on the energetics of the multibody interaction. In fact, we have found a coadsorption energy of −115.4 kcal mol^{-1}, which is about 23 kcal mol^{-1} smaller than the sum of the adsorption energies of the single reactants, amounting to −138.5 kcal mol^{-1}. Although this difference does not substantially change the energetic scenario of strongly adsorbed reacting species, the weakening of the adsorption arising from the mutual interaction of the reactants is remarkable. The coadsorption energy obtained in the present work is comparable with the one reported in refs 45 and 46, namely, −115.8 and −120.6 kcal mol^{-1}, respectively.

3.2. Acetyl Hydroxylation Reaction (Eq 1): AIMD Simulation Pathways. Considering the pivotal role of the acetyl in the rate-determining step of the EOR,[18,25,26] especially in relation to the hydroxylation reaction (eq 1), to assess the propensity of such a process in terms of mutual arrangement of the two reactants and of the reactants with respect to the Pd surface is of paramount importance. This aspect has been investigated in the present work through simulations of possible reaction pathways obtained from different initial arrangements of the reacting species.[28]

Usually, to obtain quantitative information on the energy barriers and transition states of a chemical reaction, minimum-energy path methods are employed. In this way, it is possible to obtain an energy profile as a function of some reaction coordinate, the energies of reactants and products, as well as structural and energetical insights on the reaction intermediates.[4,21,47]

As stated above, we aim instead to establish the propensity of the reaction of eq 1 from the perspective of dynamical paths produced through AIMD simulations in which acetyl and OH species are arranged above the Pd surface according to the structural information on the acetyl discussed in Section 3.1 and on the OH reported in ref 28. In particular, we opted to carry out two series of simulations, in which the initial arrangement of the acetyl is chosen in accord with the minimum-energy configurations (a) and (b) (see Figure 1). Instead, OH has been arranged in order to favor the reaction, by following simple considerations based on the chemical intuition. Therefore, as the acetic acid is formed when the hydroxyl O attacks the C_α atom, the angle between the hydroxyl H, the hydroxyl O, and the C_α atom has been set equal to 180°, while the axis containing these three atoms is nearly perpendicular to the CCO plane of acetyl. Specifically, the angle formed by the HO···C_α axis and the normal to the CCO plane is about 9.3°, being the HO···C_α axis and the normal to CCO arranged on a plane parallel to the Pd surface. The previous geometric requirements imply that the distances of the hydroxyl O and C_α atoms from the surface are equal. Ball and stick representations of the initial arrangements of the two series of simulations are shown in Figure 4. It is worth

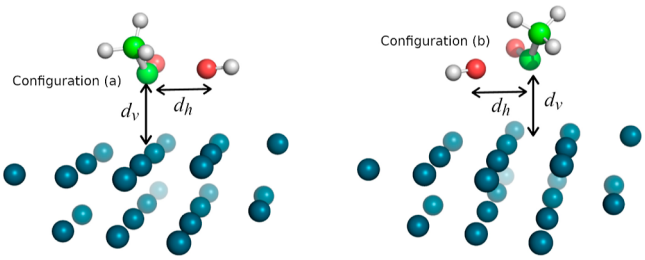

Figure 4. Ball and stick representations of the two configurations taken as initial structures for the AIMD simulations. They are based on the two minimum-energy arrangements of acetyl (Figure 1). The distance between the surface and the two reactants is indicated with d_v, while the distance between the reactants (specifically, the HO···C_α distance) is indicated with d_h. For the sake of clarity, only the first two Pd layers are displayed.

noting that, in both cases, the surface−OH energy is not expected to deviate much from the minimum energy reported in ref 28 (which amounts to ∼ − 71.3 kcal mol^{-1}). Actually, the surface-OH interaction is marginally affected by the OH orientation. In fact, the adsorption energies of different OH arrangements above the Pd surface were found greater than that of the energy-optimized structure[28] by only 10 kcal mol^{-1} or less. The symbol d_h in Figure 4 represents the distance between hydroxyl O and C_α atoms, and it can be considered as an effective distance between the two reactants. The symbol d_v indicates the distance between the OH radical (or, indifferently, the C_α atom) and the Pd surface. AIMD simulations were performed for various initial settings of the structural parameters d_v and d_h. Thus, the simulated paths are classified as reactive or nonreactive on a map of initial values of d_v, denoting the vertical shift of the acetyl-OH assembly, and d_h, denoting the horizontal shift of the reactants. These geometrical descriptors have been adopted in analogy to a previous study of the reaction $CH_3CH_2OH + OH \rightarrow CH_3CHOH + H_2O$, occurring at the Pd(111) surface.[28]

For both simulation series, namely, starting from the (a)- and (b)-type configurations, the initial d_v parameter is set to one of the following values, 1.9, 2.2, 2.5, 2.8, and 3.1 Å. Considering that for the acetyl-surface system, arranged in the

https://doi.org/10.1021/acs.jpcc.3c04587
J. Phys. Chem. C 2023, 127, 21075−21084

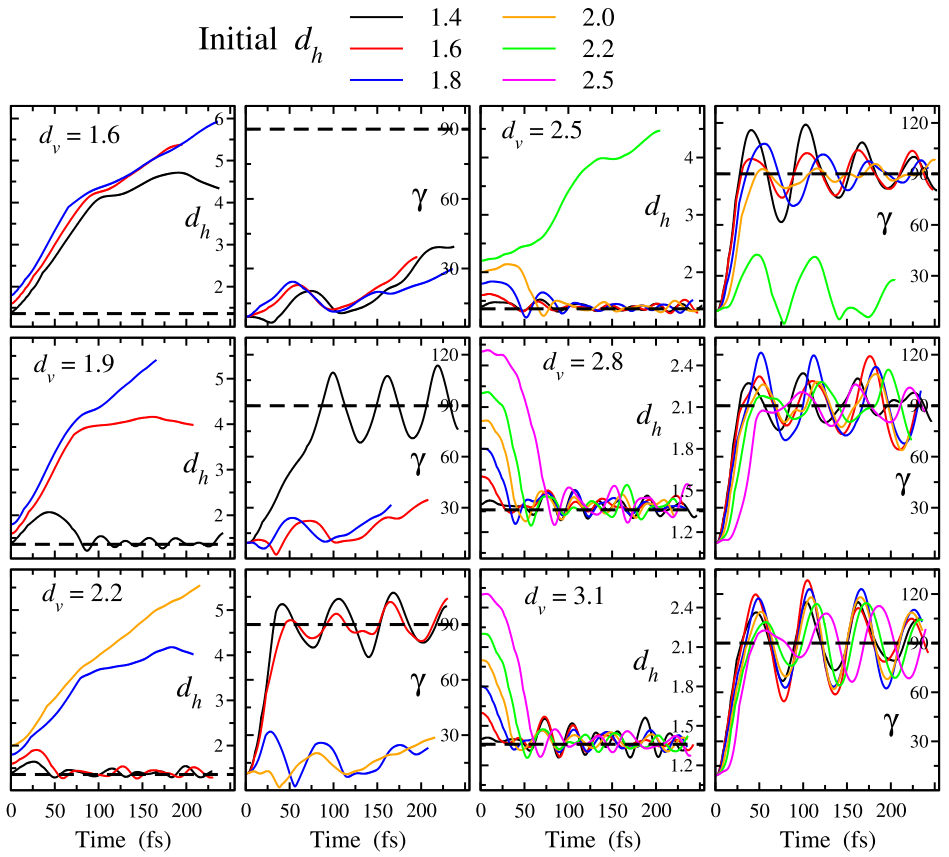

Figure 5. Time evolution of the d_h distance (in Å) and of the γ angle (in degrees) for the AIMD simulations starting from (b)-type configurations. The trajectories are classified on the basis of the initial d_v and d_h distances. In particular, the data of a panel refer to trajectories featured by the same initial d_v (reported in the panel in Å units). The various lines in a panel refer to simulations featured by different initial d_h (see the top legend). Note that the data of d_h and γ for a given initial d_v are displayed in adjacent panels. For the sake of clarity, the d_v value is specified only in the panels reporting d_h. Dashed lines denote the limit values featuring a reactive path.

(b)-type configuration, the minimum energy is observed at d_v = 1.61 Å (see Figure 2), the additional d_v value of 1.6 Å has also been considered only for the simulation series starting from the (b)-type configuration. For each d_v, the initial d_h parameter can take, in turn, the values 1.4, 1.6, 1.8, 2.0, 2.2, and 2.5 Å. Distances d_h smaller than 1.4 Å have not been considered to roughly preserve the individual molecular character of the two reacting species in the initial state of the dynamical paths. Thus, the various simulation paths differ only for the initial displacement of acetyl and OH. In particular, two generic initial configurations may differ for being the two reactants, considered as a unique assembly, rigidly shifted along the normal to the Pd(111) surface (vertical translation) and/or for being the OH molecule rigidly shifted along the HO···C_α direction, while keeping the molecular structures of OH and acetyl fixed (horizontal translation).

Actually, not all possible combinations of d_v and d_h were considered in the simulations. In fact, as we will see below, the reactivity trend classified in terms of the initial d_v and d_h parameters has a clear systematic behavior, and hence, it allowed us to make reliable predictions of some dynamical paths, without really performing the corresponding simulations. All in all, a total number of 25 and 27 AIMD trajectories have been carried out for the (a)- and (b)-type configurations, respectively.

We remark that, in all simulated paths, the initial atomic velocities are set to zero, applying a uniform down-scaling of the velocities during the simulation only when the temperature T, computed with the classical equation *kinetic energy* = $3/2Nk_BT$, where N is the number of atoms and k_B is the Boltzmann constant, exceeds an established threshold (see Section 2). We point out that this kind of calculation is addressed neither to quantify the energy barriers nor to determine optimal reaction paths but rather to evaluate if there is some evident dependence of the reactivity on the initial configuration, with special attention to the distance of the reactants from the catalyst.

The occurrence of a reactive path is probed by the time evolution of the d_h distance, which should progressively converge from the initial value to the value typical of a C_α−OH covalent bond in acetic acid, i.e., 1.32 Å.[48] As a confirmation criterion, we also checked the γ angle formed by the vector joining the C_α atom to the hydroxyl O atom and the normal to the CCO plane, pointing toward the hydroxyl O atom. In the case of a reactive path, the latter geometric descriptor should shift from 9.3° to 90°.

In Figure 5, we report the time dependence of the d_h distance and the γ angle computed for the simulations starting from the (b)-type configuration. As similar trends are obtained for the simulations starting from the (a)-type configuration, the corresponding data are not reported here. In the figure, the dashed lines indicate the limit values for d_h and γ featuring a reactive path.

According to the above-mentioned criteria, reactive and nonreactive paths are classified easily. In reactive paths, d_h and

https://doi.org/10.1021/acs.jpcc.3c04587
J. Phys. Chem. C 2023, 127, 21075−21084

Table 1. Map Reporting whether the Reaction of Eq 1 Occurs (Green Circles) or Does Not Occur (Red Circles) When the Reported d_h and d_v Distances (Å Units) Are Set in the Initial Configuration of the AIMD Simulation Paths[a]

conf. (a)	d_h 1.4	1.6	1.8	2.0	2.2	2.5
3.1	●	●	●	●	●	●
2.8	●	●	●	●	●	●
d_v 2.5	●	●	●	●	●	●
2.2	●	●	●	●	●	●
1.9	●	●	●	●	●	●

conf. (b)	d_h 1.4	1.6	1.8	2.0	2.2	2.5
3.1	●	●	●	●	●	●
2.8	●	●	●	●	●	●
2.5	●	●	●	●	●	●
d_v 2.2	●	●	●	●	●	●
1.9	●	●	●	●	●	●
1.6	●	●	●	●	●	●

[a]The outcomes refer to the simulation paths starting from (a)- and (b)-type configurations (left and right part, respectively). The pink circles identify the simulation paths, not really performed, that are predicted to be nonreactive on the basis of the general trend.

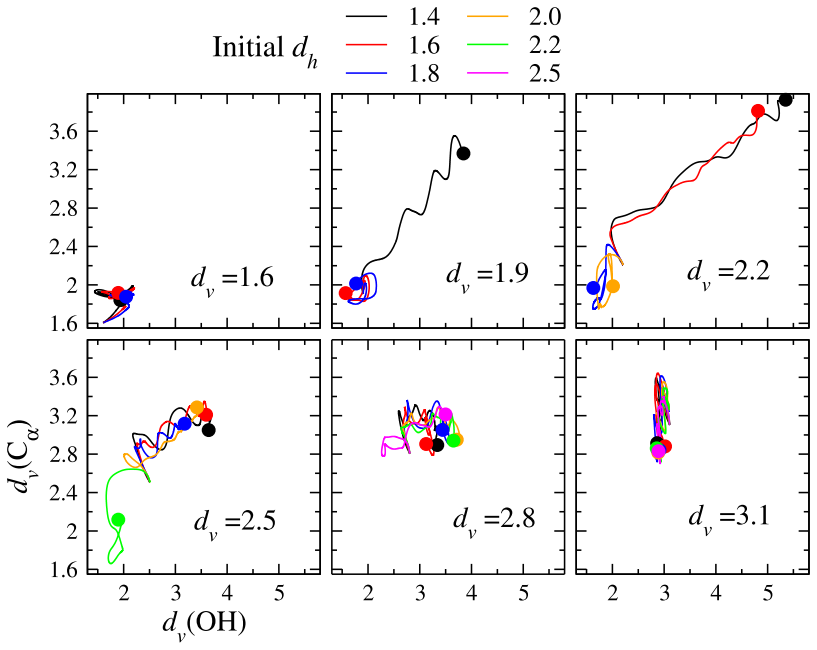

Figure 6. Time evolution of the system in the [d_v(OH), $d_v(C_\alpha)$] two-dimensional space, where d_v(OH) is the distance of the hydroxyl O from the surface and $d_v(C_\alpha)$ is the distance of the C_α atom from the surface. The trajectories are classified on the basis of the initial d_v and d_h distances (in Å). The data of a panel refer to trajectories featured by the same initial d_v values (reported in the panel). The various lines in a panel refer to different initial d_h (see the top legend). The filled circles mark the end of the simulation.

γ shift rapidly toward the limit values and then begin to fluctuate around them. Instead, in nonreactive paths, d_h shifts far away from the limit value, while γ settles on values much lower than the limit value. We point out that once the acetic acid is formed, the d_h distance and the γ angle can be associated with the CC-O stretching and COO out-of-plane bending coordinates that can be roughly exploited to assess the vibrational properties of the molecule. In this respect, in reactive paths, we do observe almost regular oscillations of these internal coordinates around their respective equilibrium values, with periods of about 30 fs (~1100 cm^{-1}) and 60 fs (~550 cm^{-1}), respectively. Even if in AIMD simulations the atomic motions are necessarily classic, the oscillations represent well the quantum mechanical behavior of the system in terms of vibrational frequencies. In fact, the frequencies reported above are fully consistent with vibrational assignments reported in either theoretical[49,50] or experimental studies.[51]

In Table 1, we report a sort of map to classify the simulated paths as reactive or nonreactive in terms of the initial values of d_h and d_v. It is worth noting that no significant differences are observed for the two series of simulations. This further supports the observations made on the adsorption energy of acetyl in the (a)- and (b)-type configurations (see Section 3.1), namely, that no preferential site, at which hydroxylation may occur, can be clearly identified. Furthermore, we note that at the d_v distances around 1.9 Å or smaller, namely, the typical distances of maximum interaction between acetyl and surface [1.93 and 1.61 Å in the (a) and (b) cases, respectively] and between OH and surface (1.62 Å; see ref 28), hydroxylation occurs only when the initial d_h distance, namely, the distance between the reactants, is as short as 1.4 Å. For d_v = 2.2 Å, the initial d_h distance of 1.6 Å or smaller allows reactivity. In order to observe reactivity for d_h values of the order of the intermolecular distances, say greater than 2 Å, d_v should be equal to or greater than 2.5 Å.

These results suggest that a strong interaction between the surface and reactants prevents hydroxylation. Conversely, hydroxylation can be observed in a much wider interval of d_h when the reactants are located far away from the surface. Therefore, the capability of the Pd surface to adsorb the reacting species has two conflicting features. On one side, it

https://doi.org/10.1021/acs.jpcc.3c04587
J. Phys. Chem. C 2023, 127, 21075−21084

fulfills the function of bringing the reacting species into contact, whereas on the other side, it plays a competitive role, hindering the reaction involving such species or intermediates.

Another interesting feature observed in the reaction paths concerns the time evolution of the distances of the reacting species, OH and acetyl, from the Pd surface. In Figure 6, we plot d_v(OH) vs d_v(C_α), namely, the distances of the hydroxyl O and C_α atoms from the Pd surface, as a function of time for the simulations starting from the (b)-type configuration. The significant aspect of the figure is that reactive and nonreactive trajectories show a very different pattern. In particular, we note that in nonreactive trajectories, the OH and acetyl molecules tend to remain strongly adsorbed to the Pd surface. In fact, the quantities d_v(OH) and d_v(C_α) are both about 2 Å, i.e., nearly the distance of the minimum-energy configuration. Instead, in reactive paths, such quantities shift far away from the optimal interaction distance or preserve the initial large values (see the cases where d_v = 2.8 and 3.1 Å in Figure 6).

These results support the hypothesis that the formation of acetic acid, or acetate in alkaline media, makes the removal of the reaction product easier owing to the low adsorption energy with respect to the acetyl and OH reactants.

From the data reported in Section 3.1, we infer that the contribution of the van der Waals interactions to the acetyl adsorption energy amounts to about 11 kcal mol^{-1}, namely, ∼ 16% of the total adsorption energy. This suggests that such interaction may play a not-so-negligible role in the acetyl hydroxylation process and hence in the EOR. To qualitatively assess how the van der Waals interactions affect the hydroxylation process, we have repeated two representative AIMD simulations (leading, in turn, to a reactive and nonreactive path) deprived of the van der Waals forces, while preserving all the other simulation settings. The time evolution of the d_h distance and γ angle obtained from these simulations is compared with that obtained from the corresponding simulations with the full potential in place. The data, reported in Section 2 of the Supporting Information, show that only negligible changes to the system trajectories are produced in the absence of van der Waals forces, supporting a scenario in which the dependence of the EOR on the dispersive forces is rather marginal.

4. CONCLUSIONS

The EOR catalyzed by Pd in alkaline media proceeds through several reaction steps, among which acetyl hydroxylation, eq 1, is the rate-determining step. In this study, we have investigated the hydroxylation process by means of quantum mechanical calculations.

We observed that the rate of the hydroxylation process depends critically on the distance of acetyl and OH from the Pd surface. In particular, we noted a rate enhancement when the distance of the two reactants from the surface increases, and hence, the adsorption strength decreases. This behavior closely relates to that recently observed on the H atom abstraction of EtOH by the OH radical.[28]

The concept that optimal performances of an electrocatalyst are obtained from a subtle balance between the requirements of having significant interactions between the reacting species and the electrode to allow electron transfer and not having an excessively strong interaction with the electrode itself in order to make such species available for the reaction is not new in electrocatalysis. This is, for example, in close correlation with the volcano-type relationship existing between the exchange current density of the H evolution reaction on monometallic surfaces in alkaline media and the H binding energy on the metal.[52,53]

An aspect that deserves an in-depth evaluation in future studies is certainly the role of the solvent in the EOR process. Although the solvent can play a relevant role in the chemical processes occurring in direct EtOH fuel cells,[54] it is often overlooked in quantum mechanical calculations, due to the large computational cost of introducing a significant number of water molecules. Concerning the intermediate reaction 1, we may speculate that the effect of the solvent is to decrease roughly the adsorption energies of the reactants,[28] eventually increasing the average distance between the surface and reactants compared to vacuum. Ultimately, this would globally enhance the propensity of reaction 1. Nonetheless, such a rate enhancement should be rather general. From a qualitative point of view, the propensity of a single hydroxylation event in the presence of a solvent, expressed in terms of the distance of the reactants from the Pd surface, is, however, expected to show some dependence on the distance itself, as revealed in the present study.

These results provide a quite robust theoretical framework for the design of Pd-based catalyst devices using, for example, light or heating of the electrode surface to selectively weaken the interactions between electrode and reacting species to eventually enhance the overall reaction rate of the EtOH electro-oxidation.

■ ASSOCIATED CONTENT

Supporting Information

The Supporting Information is available free of charge at https://pubs.acs.org/doi/10.1021/acs.jpcc.3c04587.

Additional AIMD simulation results to check the effect of the periodic boundary conditions and effect of the van der Waals interactions on the acetyl hydroxylation reaction paths (PDF)

■ AUTHOR INFORMATION

Corresponding Author

Riccardo Chelli − *Dipartimento di Chimica "Ugo Schiff", Università di Firenze, Sesto Fiorentino 50019, Italy;* orcid.org/0000-0003-3492-5709; Email: riccardo.chelli@unifi.it

Authors

Jonathan Campeggio − *Dipartimento di Chimica "Ugo Schiff", Università di Firenze, Sesto Fiorentino 50019, Italy*

Walter Giurlani − *Dipartimento di Chimica "Ugo Schiff", Università di Firenze, Sesto Fiorentino 50019, Italy*

Marco Pagliai − *Dipartimento di Chimica "Ugo Schiff", Università di Firenze, Sesto Fiorentino 50019, Italy;* orcid.org/0000-0003-0240-161X

Massimo Innocenti − *Dipartimento di Chimica "Ugo Schiff", Università di Firenze, Sesto Fiorentino 50019, Italy*

Claudio Fontanesi − *Dipartimento di Ingegneria "Enzo Ferrari", Università di Modena e Reggio Emilia, Modena 41121, Italy;* orcid.org/0000-0002-1183-2406

Complete contact information is available at: https://pubs.acs.org/10.1021/acs.jpcc.3c04587

Notes

The authors declare no competing financial interest.

https://doi.org/10.1021/acs.jpcc.3c04587
J. Phys. Chem. C 2023, 127, 21075−21084

■ ACKNOWLEDGMENTS

This research was funded by MIUR-Italy, PRIN 2017 Project (grant no. 2017YH9MRK). The authors acknowledge the CINECA award under the ISCRA initiative, for the availability of high-performance computing resources and support.

■ REFERENCES

(1) An, L.; Zhao, T. S.; Li, Y. S. Carbon-neutral sustainable energy technology: Direct ethanol fuel cells. *Renew. Sust. Energy Rev.* **2015**, *50*, 1462−1468.
(2) Zhang, S.; Shao, Y.; Yin, G.; Lin, Y. J. Recent progress in nanostructured electrocatalysts for PEM fuel cells. *J. Mater. Chem. A* **2013**, *1*, 4631−4641.
(3) Antolini, E.; Gonzalez, E. R. Alkaline direct alcohol fuel cells. *J. Power Sources* **2010**, *195*, 3431−3450.
(4) Monyoncho, E. A.; Steinmann, S. N.; Michel, C.; Baranova, E. A.; Woo, T. K.; Sautet, P. Ethanol electro-oxidation on palladium revisited using polarization modulation infrared reflection absorption spectroscopy (PM-IRRAS) and density functional theory (DFT): Why is it difficult to break the C-C bond? *ACS Catal.* **2016**, *6*, 4894−4906.
(5) Monyoncho, E. A.; Woo, T. K.; Baranova, E. A. Ethanol reaction in alkaline media for direct ethanol fuel cells. *Electrochemistry* **2018**, *15*, 1−57.
(6) Martinez, U.; Serov, A.; Padilla, M.; Atanassov, P. Mechanistic insight into oxide-promoted palladium catalysts for the electro-oxidation of ethanol. *ChemSusChem* **2014**, *7*, 2351−2357.
(7) Hu, F. P.; Chen, C. L.; Wang, Z. Y.; Wei, G. Y.; Shen, P. K. Mechanistic study of ethanol oxidation on Pd−NiO/C electrocatalyst. *Electrochim. Acta* **2006**, *52*, 1087−1091.
(8) Shen, P. K.; Xu, C. W. Alcohol oxidation on nanocrystalline oxide Pd/C promoted electrocatalysts. *Electrochem. Commun.* **2006**, *8*, 184−188.
(9) Ma, L.; Chu, D.; Chen, R. Comparison of ethanol electro-oxidation on Pt/C and Pd/C catalysts in alkaline media. *Int. J. Hydrog. Energy* **2012**, *37*, 11185−11194.
(10) Pinheiro, V. S.; Souza, F. M.; Gentil, T. C.; Parreira, L. S.; Batista, B. L.; Santos, M. C. Hybrid palladium-ceria nanorod electrocatalysts applications in oxygen reduction and ethanol oxidation reactions in alkaline media. *Int. J. Hydrog. Energy* **2021**, *46*, 15896−15911.
(11) Bellini, M.; Pagliaro, M. V.; Marchionni, A.; Filippi, J.; Miller, H. A.; Bevilacqua, M.; Lavacchi, A.; Oberhauser, W.; Mahmoudian, J.; Innocenti, M.; et al. Hydrogen and chemicals from alcohols through electrochemical reforming by Pd-CeO_2/C electrocatalyst. *Inorg. Chim. Acta* **2021**, *518*, 120245.
(12) Lu, G.; Zheng, H.; Lv, J.; Wang, G.; Huang, X. Review of recent research work on CeO_2-based electrocatalysts in liquid-phase electrolytes. *J. Power Sources* **2020**, *480*, 229091.
(13) Wang, F.; Yu, H.; Tian, Z.; Xue, H.; Feng, L. Active sites contribution from nanostructured interface of palladium and cerium oxide with enhanced catalytic performance for alcohols oxidation in alkaline solution. *J. Energy Chem.* **2018**, *27*, 395−403.
(14) Monyoncho, E. A.; Ntais, S.; Brazeau, N.; Wu, J.-J.; Sun, C.-L.; Baranova, E. A. Role of the metal-oxide support in the catalytic activity of Pd nanoparticles for ethanol in alkaline media. *ChemElectroChem.* **2016**, *3*, 218−227.
(15) Bambagioni, V.; Bianchini, C.; Chen, Y.; Filippi, J.; Fornasiero, P.; Innocenti, M.; Lavacchi, A.; Marchionni, A.; Oberhauser, W.; Vizza, F. Energy efficiency enhancement of ethanol on Pd-CeO_2/C in passive and active polymer electrolyte-membrane fuel cells. *ChemSusChem* **2012**, *5*, 1266−1273.
(16) Zhou, Z.-Y.; Wang, Q.; Lin, J.-L.; Tian, N.; Sun, S.-G. In situ FTIR spectroscopic studies of ethanol on Pd electrode in alkaline media. *Electrochim. Acta* **2010**, *55*, 7995−7999.
(17) Fang, X.; Wang, L.; Shen, P. K.; Cui, G.; Bianchini, C. An in situ Fourier transform infrared spectroelectrochemical study on ethanol on Pd in alkaline solution. *J. Power Sources* **2010**, *195*, 1375−1378.
(18) Liang, Z. X.; Zhao, T. S.; Xu, J. B.; Zhu, L. D. Mechanism study of the ethanol oxidation reaction on palladium in alkaline media. *Electrochim. Acta* **2009**, *54*, 2203−2208.
(19) Wang, E. D.; Xu, J. B.; Zhao, T. S. Density functional theory studies of the structure sensitivity of ethanol oxidation on palladium surfaces. *J. Phys. Chem. C* **2010**, *114*, 10489−10497.
(20) Sheng, T.; Lin, W.-F.; Hardacre, C.; Hu, P. Role of water and adsorbed hydroxyls on ethanol electrochemistry on Pd: New mechanism, active centers, and energetics for direct ethanol fuel cell running in alkaline medium. *J. Phys. Chem. C* **2014**, *118*, 5762−5772.
(21) Cui, G.; Song, S.; Shen, P. K.; Kowal, A.; Bianchini, C. First-principles considerations on catalytic activity of Pd toward ethanol oxidation. *J. Phys. Chem. C* **2009**, *113*, 15639−15642.
(22) Li, M.; Guo, W.; Jiang, R.; Zhao, L.; Shan, H. Decomposition of ethanol on Pd(111): A density functional theory study. *Langmuir* **2010**, *26*, 1879−1888.
(23) Guo, W.; Li, M.; Lu, X.; Zhu, H.; Li, Y.; Li, S.; Zhao, L. Ethanol decomposition on a Pd(110) surface: A density functional theory investigation. *Dalton Trans.* **2013**, *42*, 2309−2318.
(24) Sutton, J. E.; Vlachos, D. G. Ethanol activation on closed-packed surfaces. *Ind. Eng. Chem. Res.* **2015**, *54*, 4213−4225.
(25) Guo, Y.; Li, B.; Shen, S.; Luo, L.; Wang, G.; Zhang, J. Potential-dependent mechanistic study of ethanol electro-oxidation on palladium. *ACS Appl. Mater. Interfaces* **2021**, *13*, 16602−16610.
(26) Yang, Y.-Y.; Ren, J.; Li, Q.-X.; Zhou, Z.-Y.; Sun, S.-G.; Cai, W.-B. Electrocatalysis of ethanol on a Pd electrode in alkaline media: an in situ attenuated total reflection surface-enhanced infrared absorption spectroscopy study. *ACS Catal.* **2014**, *4*, 798−803.
(27) Bianchini, C.; Shen, P. K. Palladium-based electrocatalysts for alcohol oxidation in half cells and in direct alcohol fuel cells. *Chem. Rev.* **2009**, *109*, 4183−4206.
(28) Campeggio, J.; Volkov, V.; Innocenti, M.; Giurlani, W.; Fontanesi, C.; Zerbetto, M.; Pagliai, M.; Lavacchi, A.; Chelli, R. Ethanol electro-oxidation reaction on the Pd(111) surface in alkaline media: insights from quantum and molecular mechanics. *Phys. Chem. Chem. Phys.* **2022**, *24*, 12569−12579.
(29) VandeVondele, J.; Krack, M.; Mohamed, F.; Parrinello, M.; Chassaing, T.; Hutter, J. Quickstep: Fast and accurate density functional calculations using a mixed Gaussian and plane waves approach. *Comput. Phys. Commun.* **2005**, *167*, 103−128.
(30) Kühne, T. D.; Iannuzzi, M.; Del Ben, M.; Rybkin, V. V.; Seewald, P.; Stein, F.; Laino, T.; Khaliullin, R. Z.; Schütt, O.; Schiffmann, F.; et al. CP2K: An electronic structure and molecular dynamics software package - Quickstep: Efficient and accurate electronic structure calculations. *J. Chem. Phys.* **2020**, *152*, 194103.
(31) Perdew, J. P.; Burke, K.; Ernzerhof, M. Generalized gradient approximation made simple. *Phys. Rev. Lett.* **1996**, *77*, 3865−3868.
(32) Grimme, S.; Antony, J.; Ehrlich, S.; Krieg, H. A consistent and accurate ab initio parametrization of density functional dispersion correction (DFT-D) for the 94 elements H-Pu. *J. Chem. Phys.* **2010**, *132*, 154104.
(33) Goedecker, S.; Teter, M.; Hutter, J. Separable dual-space Gaussian pseudopotentials. *Phys. Rev. B* **1996**, *54*, 1703−1710.
(34) Hartwigsen, C.; Goedecker, S.; Hutter, J. Relativistic separable dual-space Gaussian pseudopotentials from H to Rn. *Phys. Rev. B* **1998**, *58*, 3641−3662.
(35) VandeVondele, J.; Hutter, J. Gaussian basis sets for accurate calculations on molecular systems in gas and condensed phases. *J. Chem. Phys.* **2007**, *127*, 114105.
(36) Arblaster, J. W. Crystallographic properties of palladium. *Platin. Met. Rev.* **2012**, *56*, 181−189.
(37) Arblaster, J. W. Crystallographic properties of platinum. *Platin. Met. Rev.* **1997**, *41*, 12−21.
(38) Momma, K.; Izumi, F. VESTA3 for three-dimensional visualization of crystal, volumetric and morphology data. *J. Appl. Crystallogr.* **2011**, *44*, 1272−1276.

https://doi.org/10.1021/acs.jpcc.3c04587
J. Phys. Chem. C 2023, 127, 21075−21084

(39) Grimme, S.; Bannwarth, C.; Shushkov, P. A Robust and accurate tight-binding quantum chemical method for structures, vibrational frequencies, and noncovalent interactions of large molecular systems parametrized for all -Block elements (Z = 1−86). *J. Chem. Theory Comput.* **2017**, *13*, 1989−2009.
(40) VandeVondele, J.; Hutter, J. An efficient orbital transformation method for electronic structure calculations. *J. Chem. Phys.* **2003**, *118*, 4365−4369.
(41) Weber, V.; VandeVondele, J.; Hutter, J.; Niklasson, A. M. N. Direct energy functional minimization under orthogonality constraints. *J. Chem. Phys.* **2008**, *128*, 084113.
(42) Bogojeski, M.; Vogt-Maranto, L.; Tuckerman, M. E.; Müller, K. R.; Burke, K. Quantum chemical accuracy from density functional approximations via machine learning. *Nat. Commun.* **2020**, *11*, 5223−5311.
(43) Pallassana, V.; Neurock, M. Reaction paths in the hydrogenolysis of acetic acid to ethanol over Pd(111), Re(0001), and PdRe alloys. *J. Catal.* **2002**, *209*, 289−305.
(44) Tereshchuk, P.; Da Silva, J. L. F. Ethanol and water adsorption on close-packed 3d, 4d, and 5d transition-metal surfaces: a density functional theory investigation with van der Waals correction. *J. Phys. Chem. C* **2012**, *116*, 24695−24705.
(45) Miao, B.; Wu, Z.-P.; Xu, H.; Zhang, M.; Chen, Y.; Wang, L. DFT studies on the key competing reaction steps towards complete ethanol oxidation on transition metal catalysts. *Comput. Mater. Sci.* **2019**, *156*, 175−186.
(46) Wu, Z.-P.; Miao, B.; Hopkins, E.; Park, K.; Chen, Y.; Jiang, H.; Zhang, M.; Zhong, C.-J.; Wang, L. Poisonous species in complete ethanol oxidation reaction on palladium catalysts. *J. Phys. Chem. C* **2019**, *123*, 20853−20868.
(47) Sheng, T.; Wu, H.-Y.; Lin, X.; Lin, W.-F. Insights into reaction mechanisms of ethanol at the Pt/Au(111) interfaces using density functional theory. *Phys. Chem. Chem. Phys.* **2022**, *24*, 27277−27288.
(48) Boese, R.; Bläser, D.; Latz, R.; Bäumen, A. Acetic acid at 40K. *Acta Crystallogr.* **1999**, *C55*, IUC9900001.
(49) Turi, L.; Dannenberg, J. J. Molecular orbital study of acetic acid aggregation. 1. Monomers and dimers. *J. Phys. Chem.* **1993**, *97*, 12197−12204.
(50) Burneau, A.; Génin, F.; Quilès, F. Ab initio study of the vibrational properties of acetic acid monomers and dimers. *Phys. Chem. Chem. Phys.* **2000**, *2*, 5020−5029.
(51) Haurie, M.; Novak, A. Spectres de vibration des molécules CH_3COOH, CH_3COOD, CD_3COOH et CD_3COOD. *J. Chim. Phys.* **1965**, *62*, 137−145.
(52) Sheng, W.; Myint, M.; Chen, J. G.; Yan, Y. Correlating the hydrogen evolution reaction activity in alkaline electrolytes with the hydrogen binding energy on monometallic surfaces. *Energy Environ. Sci.* **2013**, *6*, 1509−1512.
(53) Zheng, J.; Nash, J.; Xu, B.; Yan, Y. Perspective—Towards Establishing Apparent Hydrogen Binding Energy as the Descriptor for Hydrogen Oxidation/Evolution Reactions. *J. Electrochem. Soc.* **2018**, *165*, H27−H29.
(54) Wu, R.; Wang, L. Insight into the solvent effects on ethanol oxidation on Ir(100). *Phys. Chem. Chem. Phys.* **2023**, *25*, 2190−2202.

https://doi.org/10.1021/acs.jpcc.3c04587
J. Phys. Chem. C 2023, 127, 21075−21084